# Chassis Design of Tomato Picking Robot in the Greenhouse



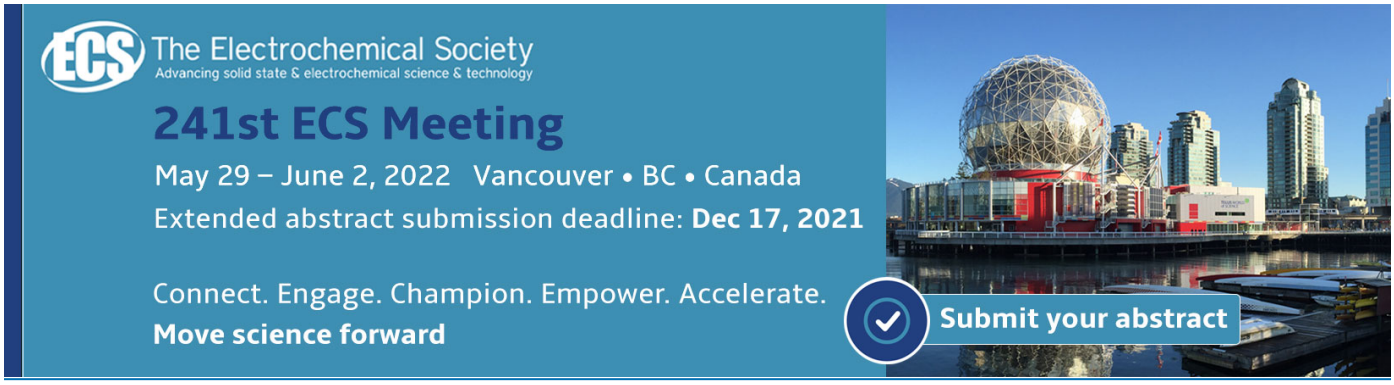

# Chassis Design of Tomato Picking Robot in the Greenhouse

**Tao Zhu*, JinHua Xiang**

Northwest A&F University, Shanxi, China

*Corresponding author's e-mail: zhutao@nwafu.edu.cn

**Abstract.** At present, the artificial fruit picking cost is high, the fruit damage rate is high, and the efficiency is low, so the greenhouse picking robot emerges as the times' demand. Therefore, this paper designs a kind of a chassis system of greenhouse picking robots. This paper mainly designed and simulates the chassis mechanical system, electrical system, and basic motion control algorithm from three aspects. Finally, the prototype of the chassis system of the picking robot in the greenhouse is completed and the chassis system is debugged, which proves that it has the characteristics of adaptability to the greenhouse environment, strong universality, and strong expansibility.

## 1. Introduction

At present, the robots research mostly focuses on the detection of the robot arm, end-effector, and related sensors, while the research on robot chassis is relatively few. As an important part of the picking robot, the research on the chassis of the picking robot is conducive to the complete construction of the mechanical system of the picking robot and the improvement of the performance of the robot picking operation [1].

In this paper, the wheel chassis driven by DC motor is designed for tomato picking operation in the greenhouse, including mechanical system, electrical system, and basic motion control algorithm, which is helpful to improve the performance of the picking robot.

## 2. Overall design of chassis

Generally speaking, the row spacing of greenhouse tomatoes is 80-90cm [2], so the structure of the greenhouse tomato picking robot chassis should be miniaturized and simplified to facilitate the installation of mechanical arms and sensors. After comprehensive consideration, the robot chassis performance parameters are shown in Table 1.

Tab. 1 Robot performance parameters

| parameter | size | speed | Steering radius | power | load |
|---|---|---|---|---|---|
| indicators | 1000×500×365mm3 | 5~6 m/s | 65cm | 50 W | 60 kg |

The chassis system of the picking robot includes a chassis girder, front and rear wheels, and suspension, driving transmission system, chassis shell, and electrical control system, etc. [3], as shown in Figure 1. The chassis girder is the backbone of the whole chassis, located in the middle

layer, above which is the picking system installation seat, shell, and fruit collection device, the lower part is the control system installation area. A navigation system mounting seat is arranged above the car head end of the shell, and a plurality of navigation devices can be installed.

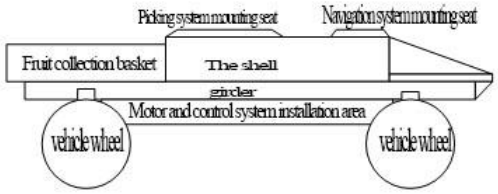


**Fig. 1** Picking robot chassis architecture

## 3. Mechanical structure design

Greenhouse picking robot chassis using four-wheel chassis scheme, wheel suspension selection swing shaft suspension. The chassis frame is the mechanical structure foundation of the chassis system, which is divided into three parts: the installation frame of the picking system, the girder assembly, and the auxiliary structural parts. The overall structure is shown in Figure 2.

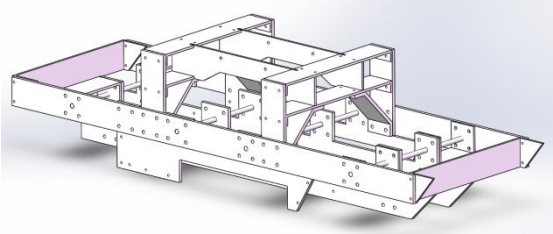

**Figure 2.** Chassis frame

### *3.1. Installation rack of picking system*

The mounting frame of the picking system consists of a quick disassembly mounting seat, bracket, transverse beam, longitudinal beam, and supporting beam, as shown in Fig. 3. The quick disassembly mounting seat is a load-bearing plate with a quick disassembly function. If the maximum size of the base allows, other equipment can be installed directly on the user interface, which improves the versatility of the chassis system.

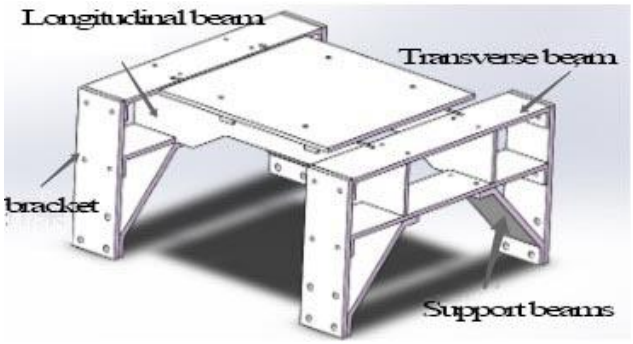


**Fig. 3** Mounting frame of picking system

The design of longitudinal beam is to directly bear the load applied by the quick removal mounting seat, so to improve the load-bearing capacity, its cross-section is designed as a vertical narrow rectangle. The longitudinal beam thickness is 4mm. The two ends are slightly reduced in width so that they can be inserted exactly between the two transverse beams, as shown in Fig. 4, Part A. At the same time, the area corresponding to the installation position of the longitudinal beam on the two transverse beams is provided with a clamping slot whose width is equal to the thickness of the longitudinal beam, so that the two points of the longitudinal beam A and B can precisely clamber into the clamping slot. In this way, the longitudinal beam on the transverse beam installation without bolts and other fasteners, to avoid axial rotation.

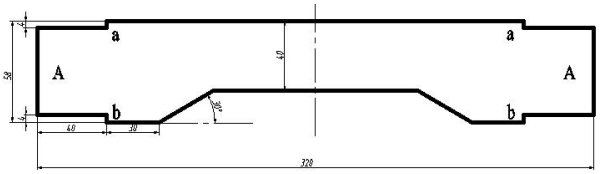


**Fig. 4** Dimensions of longitudinal beam

Because the longitudinal beam is the main load-bearing part, the mechanical strength should be checked. Suppose that the middle section of the longitudinal beam is subjected to the uniform load of 200mm × 4mm, the side of the longitudinal beam is axisymmetric, and both ends are subjected to the uniform load of 40mm × 4mm. It is known that the supporting force of each longitudinal beam on the mounting seat is 300N, so the uniform load of the middle section is

$$q_L = \frac{F}{200mm} = \frac{300N}{200mm} = 1500N/m \tag{1}$$

If the force system is simplified to the middle point, there is

$$\begin{cases} q_L \times 200mm = q_{N1} \times 40mm + q_{N2} \times 40mm \\ q_{N1} \times 140mm = q_{N2} \times 140mm \end{cases} \tag{2}$$

Can solve qN1=qN2=3750N/m。

The cross section of the whole member is divided into five cases A~E, and the cross-section parameters of each case are listed after calculation, as shown in Table 2.

**Tab. 2** Parameters of cross section of each section

| | A | B | C | D | E |
|---|---|---|---|---|---|
| Width b(m) | 4×10-3 | 4×10-3 | 4×10-3 | 4×10-3 | 4×10-3 |
| Thickness h(m) | 0.05 | 0.058 | 0.058 | 0.058-0.577x | 0.04 |
| Area S(m2) | 2×10-4 | 2.32×10-4 | 2.32×10-4 | 2.32×10-4-2.308x | 1.6×10-4 |
| Bending section coefficient W(m3) | 1.66×10-6 | 2.24×10-6 | 2.24×10-6 | (2.22x2-4.46x+0.0224)×10-4 | 1.0×10-6 |
| note | The x in column D is in the range 0≤x≤0.0312m | | | | |

The shear force diagram and bending moment diagram of the longitudinal beam can be calculated and drawn, as shown in Fig. 5.

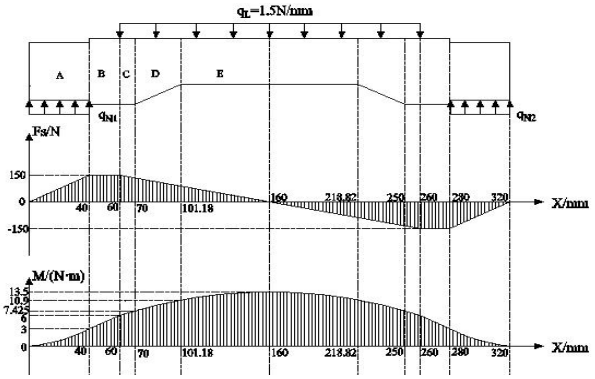


**Fig. 5** Tensile force diagram, shear force diagram and bending moment diagram

In section D, the cross-sectional area decreases linearly, but because the bending moment increases monotonically, the maximum value of normal stress also increases monotonically. However, both the shear force and the cross-sectional area decrease, so it is impossible to see the change rule of shear stress directly. Therefore, it is necessary to carry out relevant calculations.
When the cross section is a rectangle, the maximum shear stress formula on it is

$$\tau_{MAX} = \frac{3}{2} \cdot \frac{F_S}{bh} \tag{3}$$

In segment D, FS and (BH) are represented by X, which are

$$\begin{aligned} F_S &= 135 - 1.5X \\ bh &= 232 - 2.309x (0 \le x \le 31.177, \text{ Unit of mm}) \end{aligned} \tag{4}$$

Substitute the system of equations (4) into Equation (3) to obtain

$$\tau_{MAX} = \frac{3}{2} \cdot \frac{135 - 1.5\text{x}}{232 - 2.309\text{x}} (0 \le \text{x} \le 31.177\text{mm}) \tag{5}$$

Derivation shows that function 3-3 is a decreasing function in its definition domain, so the cutting strain diagram can be drawn as shown in Fig.6.

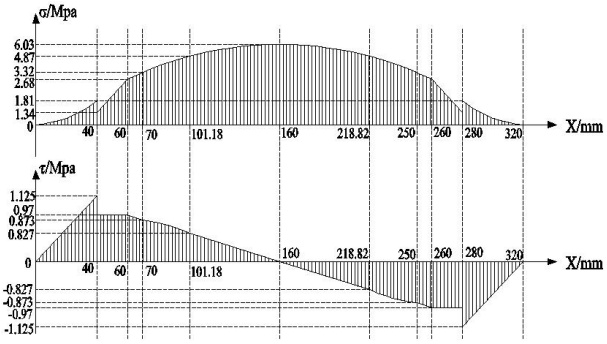


**Fig. 6** Normal stress diagram and shear stress diagram

It can be seen that the longitudinal beam satisfies

$$\begin{cases} \sigma_{MAX} < [\sigma] \\ \tau_{MAX} < [\tau] \end{cases} \tag{6}$$

Therefore, the strength of the longitudinal beam meets the requirements.

### *3.2. Girder assembly*

The girder assembly is the backbone of the entire chassis mechanical system, on which all mechanical structures are mounted [4], as shown in Fig. 7. The structure assembly mainly includes "four-axis six beams". Four transverse through-shafts provide vertical support for the girder to withstand loads. Also, several auxiliary structural parts between each structural beam play a role in positioning and supporting each structural beam to ensure the robustness and stability of the whole girder assembly, as shown in Fig. 8.

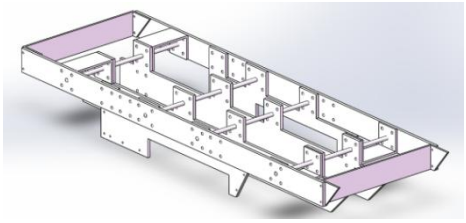

**Fig. 7** Girder assembly

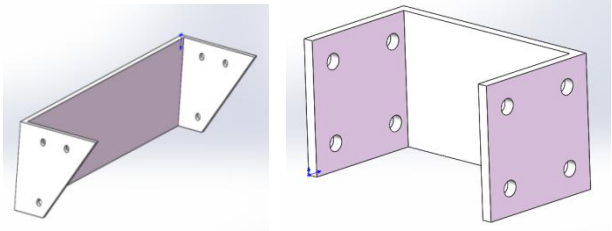

(a) b)

**Fig. 8** Various auxiliary structural parts

## 4. Drive the driveline

In this paper, the picking robot chassis system adopts XD-60GA775 DC reducer motor as the source of driving power. The rated voltage of the motor is 12V, and the rated speed is 10r/min.

The force analysis of the rear wheel is shown in Fig. 9. If the horizontal direction to the right is the driving direction, then Me is the maximum driving torque of the motor, FL is the vertical force of the chassis on the wheels, F is the horizontal force of the chassis on the wheels, Fn is the support force of the ground on the wheels, and F is the ground friction force of the wheels. According to the force analysis, the conditions under which the wheel can rotate under the action of the motor driving torque are

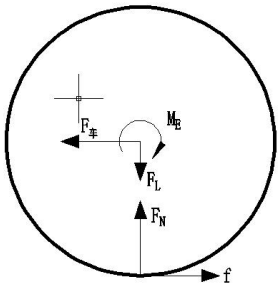


**Fig. 9** Mechanical analysis of wheel

$$\begin{cases} F_{车} = \mathrm{f} \\ \mathrm{F_L} = \mathrm{F_N} \\ \mathrm{M_E} \le \mathrm{f} \times \mathrm{r} \\ \mathrm{f} = \mu \times \mathrm{F_N} \end{cases} \tag{7}$$

Where, r is the wheel radius, r=90mm, μ is the static friction coefficient between the wheel and the ground.

Referring to the motor parameter table, it can be seen that the maximum torque of the type with the maximum speed of 10r/min in this series of reducer motors is 76.4kgf /cm [5]. Assume that the load condition of chassis is the maximum load state, that is, the load is 60kg, the dead weight of the vehicle is 20kg, then

$$F_L = \frac{1}{4} \times (60 + 20) \times 9.8 = 196N \tag{8}$$

So we can solve for that μ⩽0.43。

Assuming that the chassis load is in the medium load level, namely, the load of 30kg, can be calculated μ⩽0.69. According to the relevant information, the static friction coefficient between the wheel and the dirt road surface is about 0.5~0.7[5]. It can be seen that the chassis can maneuver on the greenhouse soil pavement under the condition of the medium load.

To prevent dust from the dirt road surface from adversely affecting the motor, an electric engine room is designed in the chassis girder assembly, and the chassis shell is added for the chassis system, as shown in Fig. 10 and 11.

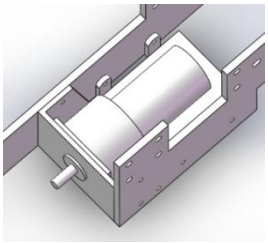

**Fig. 10** Electrical machinery room and motor installation

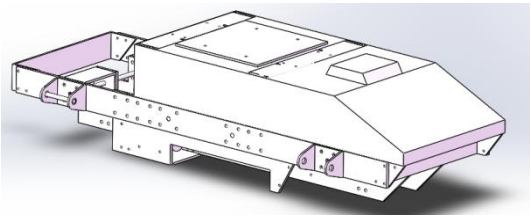

**Fig. 11** Installation effect of upper enclosure

## 5. Electrical system design

The electrical system is the control core of the robot chassis, which is used to observe and feedback the environmental conditions around the robot and control the robot chassis to complete specific actions [6]. It mainly includes two parts: the power supply circuit and the control circuit.

In order to improve the versatility of the chassis, the control instructions of the chassis should be as simple as possible. This paper uses the way of the parallel bus to establish the user's upper computer to control the chassis master chip STM32F103ZET6 microcontroller, as shown in Figure

12. The parallel bus is composed of eight Dupont lines, numbered 0~7, of which 0~3 are mode selection lines. By permutation and combination of high and low levels, 16 combination ways are matched to represent different actions or action groups. Line 4~6 is the gear selection line. The three lines are matched with eight combinations to represent eight driving speeds and eight steering angles when steering. Line 7 is a "progressive switch". When it inputs a high level, the controlled speed and steering Angle will gradually increase from zero to the set value, while when it inputs a low level, the controlled speed and steering Angle will change in the form of step input.

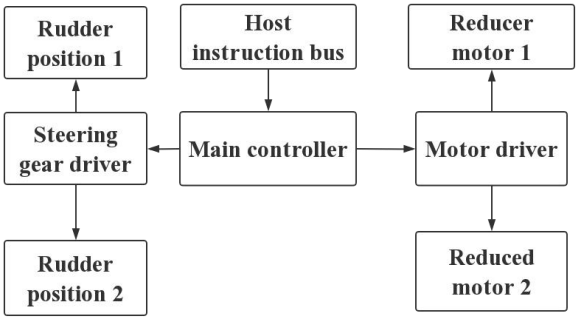


**Fig. 12** Control circuit architecture

The power supply circuit is used to provide power for the control circuit and the actuator to ensure its normal operation. It is composed of 12V high voltage power supply, 7.4V low voltage power supply, manual switch and 12V-5V voltage regulator module, as shown in Fig. 13. This part of the circuit is responsible for providing various required voltages for the control circuit and the actuator.

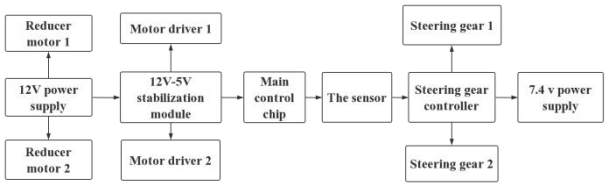


**Fig. 13** Power supply circuit architecture

Control program design

The whole control program adopts the structure of "initialization-main loop", that is, the components in the main control chip are initialized first, and after the initialization, the program enters an endless cycle of repeated execution, repeat a series of steps, such as receiving instructions, performing actions, and detecting the environment. The general flow chart of the control program is shown in figure.

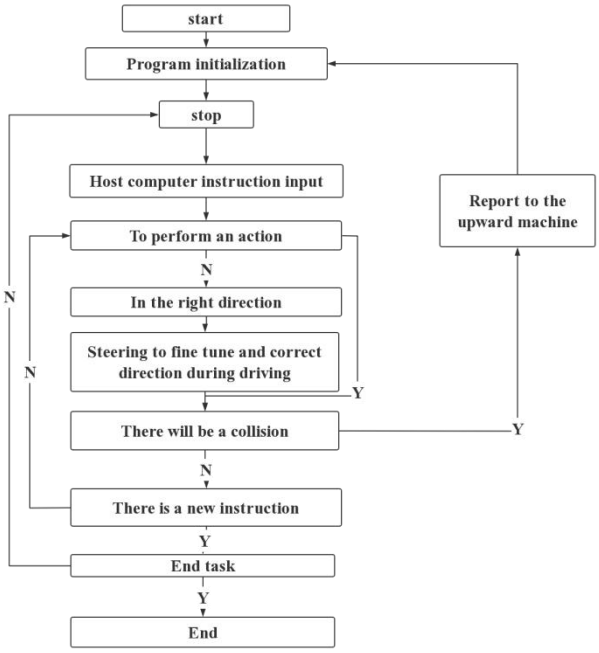


**Fig. 14** Control program flow chart

For the convenience of description, the four wheels of the picking robot chassis are numbered, as shown in Fig. 14, and the forward rotation of the wheels is defined as positive rotation, and the backward rotation is defined as reverse rotation.

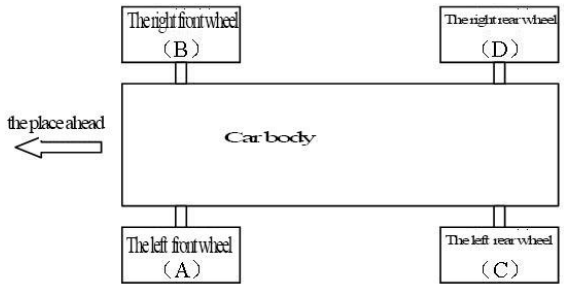


**Fig. 15** Wheel number

According to the communication protocol between the user's upper computer and the master control chip, the 0-3 bits of the instruction receiving bus are the mode selection lines, and the corresponding actions of different signal combinations are shown in Table 3. The undefined signal combination cannot control the movement but can be used for the subsequent development of the chassis movement function.

**Tab. 3** Different control signals and their corresponding actions

| No. 0 | No. 1 | No. 2 | No. 3 | The corresponding action |
|---|---|---|---|---|
| 0 | 0 | 0 | 0 | parking |

| | | | | |
|---|---|---|---|---|
| 0 | 0 | 0 | 1 | forward |
| 0 | 0 | 1 | 0 | back |
| 0 | 0 | 1 | 1 | Turn left in situ |
| 0 | 1 | 0 | 0 | In situ turn right |
| 0 | 1 | 0 | 1 | Turn left in situ |
| 0 | 1 | 1 | 0 | In situ turn right |
| 0 | 1 | 1 | 1 | Turn left in situ |
| 1 | 0 | 0 | 0 | In situ turn right |
| 1 | 0 | 0 | 1 | undefined |
| 1 | 0 | 1 | 0 | undefined |
| 1 | 0 | 1 | 1 | undefined |
| 1 | 1 | 0 | 0 | undefined |
| 1 | 1 | 0 | 1 | undefined |
| 1 | 1 | 1 | 0 | undefined |
| 1 | 1 | 1 | 1 | undefined |

For forward and backward, the speed is divided into eight gears from zero to the maximum. When the master chip receives different signals from the 4th to 6th bits of the instruction receiving bus, different speed values can be determined. The maximum speed of the reducer motor is 10r/min, and the wheel diameter is 180mm, so the maximum driving speed

$$v_{\max} = 10 \times 2\pi(\frac{d}{2}) = 10 \times 2\pi \times 0.09 \approx 5.6m/s \tag{9}$$

The corresponding relationship between the speed tap position and the 4th to 6th bit control signals of the instruction bus is shown in Table 4. The speed can also be linearly increased or decreased when the seventh bit, the "progressive switch", is input to a high level.

**Tab. 4** Different control signals and their corresponding speed values

| No .4 | No .5 | No.6 | Velocity (m/s) |
|---|---|---|---|
| 0 | 0 | 0 | 0 |
| 0 | 0 | 1 | 0.8 |
| 0 | 1 | 0 | 1.6 |
| 0 | 1 | 1 | 2.4 |
| 1 | 0 | 0 | 3.2 |
| 1 | 0 | 1 | 4.0 |
| 1 | 1 | 0 | 4.8 |
| 1 | 1 | 1 | 5.6 |

When the chassis turns in place, the two rear wheels rotate equally and in opposite directions. When the chassis turns left in situ, wheel C reverses and wheel D turns forward. When the chassis turns right in situ, wheel C turns forward and wheel D reverses.

The maximum angular velocity was set as 180° /s, and the available angular velocity was divided into five values from zero to 180° /s according to the communication protocol. The corresponding relationship between the angular velocity value, its control signal and wheel speed are shown in Table 5. When the seventh "progressive switch" input is high, the angular velocity can be linearly increased or decreased.

The chassis is steered by Ackerman's steering principle, and the two front wheels are driven by two steering gear, so the steering Angle of the two front wheels can be controlled independently. For example, the principle of Ackermann turning is shown in Fig. 16.
When the chassis is in Ackerman steering, it is known from the data in Table 5

$$\alpha = \arctan\frac{AC}{OC} = \arctan\frac{AC}{OM - MC} = \arctan\frac{625}{R - 180} \tag{10}$$

$$\beta = \arctan\frac{BD}{OD} = \arctan\frac{BD}{OM + MD} = \arctan\frac{625}{R + 180} \tag{11}$$

**Tab. 5** Different angular velocity values and their corresponding control signals and wheel speed

| angular velocity value (/ s) | No .4 | No .5 | No.6 | Velocity value (m/s) |
|---|---|---|---|---|
| 0 | 0 | 0 | 0 | 0 |
| 22.5 | 0 | 0 | 1 | 0.089 |
| 45 | 0 | 1 | 0 | 0.178 |
| 67.5 | 0 | 1 | 1 | 0.267 |
| 90 | 1 | 0 | 0 | 0.356 |

It can be seen from Equations (10) and (11) that the lateral rotation Angle of the front wheel near the steering center is larger, that is, as shown in Fig. 16, there is always $\alpha > \beta$. In the chassis system in this paper, the maximum front-wheel rotation Angle is 54°, according to which the minimum steering radius can be calculated as

$$R_{\min} = 180 + \frac{625}{\tan 54^{\circ}} \approx 650\text{mm} \tag{12}$$

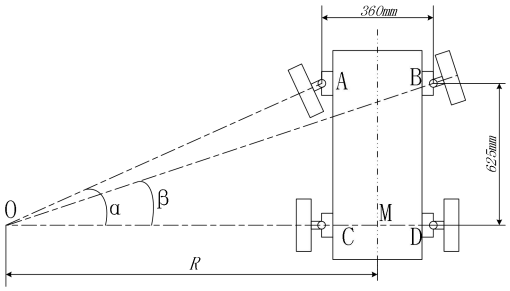


**Fig. 16** Ackermann steering principle

In this paper, the speed of the far-end rear wheels is set as 0.5m/s when the chassis runs between steering. According to the communication protocol, the steering radius of the chassis is divided into eight gears from 650mm to 1000mm, and the driving speeds of the far and near rear wheels corresponding to each gear, as well as the corresponding α and β in this case, are shown in Table 6.

**Tab. 6** various inter-run steering conditions

| Gear signal | Steering radius (m) | Distal rear wheel speed (m/s) | Proximal rear wheel speed (m/s) | α angle values(°) | β angle value(°) |
|---|---|---|---|---|---|

| | | | | | |
|---|---|---|---|---|---|
| 000 | 0.65 | 0.5 | 0.362 | 53.05 | 36.95 |
| 001 | 0.70 | 0.5 | 0.371 | 50.25 | 35.38 |
| 010 | 0.75 | 0.5 | 0.380 | 47.50 | 33.90 |
| 011 | 0.80 | 0.5 | 0.388 | 45.25 | 32.50 |
| 100 | 0.85 | 0.5 | 0.394 | 43.00 | 31.25 |
| 101 | 0.90 | 0.5 | 0.400 | 41.00 | 30.05 |
| 110 | 0.95 | 0.5 | 0.405 | 39.05 | 28.95 |
| 111 | 1.00 | 0.5 | 0.410 | 37.32 | 27.90 |

The case of reverse left turns, and reverse right turn is similar to the case of a forward left turn and forward right turn, so it will not be specifically described.

When the "stop" command is received, the motors on all four wheels slow down and stop at the same time, thus achieving the purpose of braking. The stop command can be divided into two modes: urgent stop and slow stop. When the stop command is issued, if the "progressive switch" is at a high level, the slow stop mode will be triggered. The chassis will start from the current driving speed and reduce the speed to zero evenly within a certain time interval. If the "progressive switch" is low, an emergency stop mode is triggered, and the chassis immediately stops the motor to achieve an emergency stop.

## 6. To summarize

Taking the greenhouse tomato picking as an example, this paper designs a greenhouse picking robot chassis system by analyzing the environment and mode of greenhouse tomato planting. The chassis system has many kinds of general-purpose actuator interfaces, which can adapt to the greenhouse environment, has strong universality and expansibility, and achieves the goal of “Being able to go to ground” and “Versatile”.

## References

[1] Chen, Y. B., Liu, L. J. (2015) Research on teaching reform based on robot competition [J]. Education and Teaching Forum, (21):123-124.
[2] Zhang, Z. Z. (2016) Review of Wheeled Mobile Robot Research [J]. Electronic Technology and Software Engineering, (23):120.
[3] Wang, Y., Zhang, X. J., Shi, Y. G. (2019) UWB/gyroscope combination of greenhouse spray robot navigation system design [J]. Information Technology and Information Technology, (06):60-62.
[4] Zhang, S. H., Liu, F., Liu, L., Shi, Y, G. (2018) Design of Orchard Spray Robot for Competition [J]. Mechanical Engineering and Automation, (2):153-156.
[5] Wan, B., Wang, D., Shi, Y. H. (2018) Design of Intelligent Tracking Car System Based on STM32F103 Controller [J]. Industrial Control Computer, 31(06):137-139.
[6] Zheng, J. H., Li, J. (2020) Dynamic Wireless Charging System of Electric Car Based on STM32 [J]. Software, 41(01):240-244.